THE USE OF MICROSTRUCTURE SIMULATION AND A PATTERN MATCHING LIBRARY METHOD FOR EBSD GRAIN SIZE MEASUREMENT ANALYSIS

BY

YURI AMORIM COUTINHO

A THESIS
SUBMITTED TO THE FACULTY OF

ALFRED UNIVERSITY

IN PARTIAL FULFILLMENT OF THE REQUIREMENTS
FOR THE DEGREE OF

MASTER OF SCIENCE

IN

MATERIALS SCIENCE AND ENGINEERING

ALFRED, NEW YORK

MAY, 2016

THE USE OF MICROSTRUCTURE SIMULATION AND A PATTERN MATCHING LIBRARY METHOD FOR EBSD GRAIN SIZE MEASUREMENT ANALYSIS

BY

YURI AMORIM COUTINHO

B.S. RIO DE JANEIRO STATE UNIVERSITY (2014)

SIGNATURE OF AUTHOR_____

APPROVED BY_____

DAVID W. LIPKE, ADVISOR

_____

S. K. SUNDARAM, ADVISORY COMMITTEE

_____

STEVEN C. TIDROW, ADVISORY COMMITTEE

_____

CHAIR, ORAL THESIS DEFENSE

ACCEPTED BY_____

DOREEN D. EDWARDS, DEAN
KAZUO INAMORI SCHOOL OF ENGINEERING

ACKNOWLEDGMENTS

I would first like to thank my advisors Dr. Eric Payton and Dr. David Lipke of the Inamori School of Engineering at Alfred University. They consistently allowed this paper to be my own work, but steered me in the right direction whenever they thought I needed it. I also would like to thank the members of my advising committee for all the feedback provided towards the completion of my degree. As well as my office and research group colleges for teaching and helping me with my research and for all Alfred University employees for always been kind and willing to help me.

To the friends I left in Alfred, my deepest regards, thank you all for being my family for these long two years. And finally I must express my very profound gratitude to my parents and to my brother for providing me with unfailing support and continuous encouragement throughout my years of study and through the process of researching and writing this thesis. This accomplishment would not have been possible without them.

TABLE OF CONTENTS

LIST OF TABLES

Page

LIST OF FIGURES

ABSTRACT

Grain size data from electron backscatter diffraction (EBSD) maps is often reported as the circle equivalent diameter of the measured grain area. Circle equivalent diameters are not directly comparable to the lineal intercept measurements historically employed for grain size measurements obtained via optical microscopy. While the value of mean lineal intercept is the same in 2D and 3D, the 2D circle equivalent section diameter is not directly related to any 3D property. Estimation of mean lineal intercept from circle equivalent diameter is usually carried out by assuming feature circularity, despite the obvious corners that are inherent to grains from the requirements of space filling. A direct conversion between section areas and lineal intercepts can be performed if the grain perimeters are known. In the present work, a novel pattern-matching library approach is investigated for measurement of grain perimeters on simulated 2D EBSD maps. The results are compared to alternative approaches for perimeter measurement and assessed with respect to spatial resolution, grain size distribution parameters, and relevant ASTM and ISO measurement standards. The benefits and drawbacks of each approach are discussed.

INTRODUCTION

Many mechanical, electrical, and magnetic properties of materials are intrinsically related to the grain size in the microstructure. The Hall-Petch relationship, which empirically correlates the grain size with yield strength, is a classic example of this dependence [1,2]. Grain size plays a significant role in many key phenomena in materials processing and performance, including creep response [3,4], flow stress during forming operations [5], phase transformations [6] and propagation of fatigue cracks [7]. Mechanical and functional properties are often improved by grain size refinement [8–12]. Hence, reliable and accurate methods to measure grain size are essential in engineering of new materials technologies as well as understanding reproducibility and variability in materials processing.

A. Grain Size Measurement

Grain boundaries are conventionally revealed by electrochemical, thermal, and/or chemical etching on a polished cross-section of material. The etched surfaces can then be digitally imaged using optical microscopy or scanning electron microscopy (SEM) based techniques. An SEM-based technique that is becoming increasingly common is electron backscatter diffraction (EBSD), where an electron beam is rastered across the surface of a tilted specimen and a high speed camera captures images of the diffraction patterns that form when the backscattered electrons hit a phosphor screen. EBSD data is collected serially on a square or hexagonal grid and can be plotted as a map of crystal orientation or phase. The principle benefit of EBSD grain size measurement over imaging of etched surfaces is the potential for reduced ambiguity about what observed feature constitutes a grain boundary, as a grain boundary in EBSD data can be identified in most cases by a sudden change in crystal orientation.

Since EBSD maps are equivalent to a grid-based digital image, grain areas as measured by point counting are a natural choice for grain size characterization in techniques such as EBSD. The grain microstructure is typically segmented in the spatially resolved EBSD orientation data using a percolation approach. The calculation is

initiated by assigning a measurement point in one corner of the scan as a member of grain #1. The crystal misorientation between the seed point and its neighbors is checked, and it is assumed that the adjacent pixel is a member of a different grain if the angular portion of the misorientation is greater than a threshold value. This process is iterated for all pixels in the scan to cluster the data into a set of grains. The area of each grain may then be calculated by summing the number of pixels assigned to that grain and multiplying by the area of a pixel, determined from the calibration parameters of the SEM.

B. Standards Review

Several standards exist for measurement of grain size from EBSD data and conventional microscopy techniques. ASTM E112-10[13], one of the most commonly used and extensive standards, describes three basic measurement methods: direct comparator, planimetric, and intercept-based procedures. The direct compactor method is semi-qualitative and prone to user judgment error. The planimetric (or Jeffries) procedure consists of a weighted count of the number of grains residing in a test circle of known area. Grains wholly within the test circle are counted with a weight of unity and grains intersected by the test line (i.e. those which lie partially inside the test circle) are weighted as one-half. The magnification must be chosen such that the test area includes at least 50 grains, and the final result is multiplied by a factor dependent on the magnification. This value is then divided by the circle area to give the number of grains per unit area N_A. Finally, the intercept procedures (attributed to Heyn [14] and Hilliard [15]) are based on the number of intersections between test lines of known length and grain boundaries. Choice of magnification and test line length should result in at least 50 intercepts. The number of intercepts with all test lines is recorded as N_I. Dividing by the total length of test lines l, a value is obtained for the mean lineal intercept ($\bar{L} = l/N_I$).

The ASTM method then converts this result into a unitless "grain size number," G. The ASTM grain size number follows a logarithmic scale of the number of grains per unit area intersected by a test plane, facilitating comparison of expected differences in properties between materials with different microstructures. The original definition of G was the base-2 logarithm of the number of grains per square inch observed in cross section at 100X magnification. The mean intersection area $\bar{A}$ is equal to $1/N_A$, thus for $\bar{A}$

measured in μm^2 at 1X magnification (i.e. using the scale bar of the image to determine the actual areas of the grain sections), the ASTM grain size can be calculated as:

$$G = (6.97737 - 3.32193\, log_{10}\, \bar{A}) \pm 10^{-5} \quad (1)$$

The reader should note that ASTM E112 only provides G conversion equations for grain areas measured in mm^2 and lineal intercepts measured in mm. For convenience, the equations presented here are for direct conversion from units of μm^2 and μm, respectively, which are more common for EBSD measurements.

Since the number of grains intercepted per unit area cannot be converted to the mean lineal intercept without additional information, there is no direct mathematical relationship between the mean lineal intercept and the ASTM grain size. ASTM E112 provides an estimate for measurements performed using the lineal intercept approach, $G \cong 2\log_2(32/\bar{L})$, for $\bar{L}$ in inches at 100X. For $\bar{L}$ measured in microns at 1X, this results in:

$$G \cong (16.64386 - 6.64386\, log_{10}\, \bar{L}\,) \pm 10^{-5} \quad (2)$$

For circles, there is an exact relationship between $\bar{L}$ and $\bar{A}$:

$$\bar{L} = \left(\frac{\pi}{4}\, \bar{A}\right)^{\frac{1}{2}} \quad (3)$$

It is not yet well characterized how much G estimated from $\bar{L}$ deviates from G determined exactly from $\bar{A}$ for realistic space filling grain shapes rather than circles.

The EBSD technique-specific ASTM standard, E2627[16], generally builds upon the foundation of E112 but differs from the parent standard in a few key ways. First, E2627 requires grains with sectional areas consisting of fewer than 100 px to be excluded from the measurement. Second, twin boundaries are to be excluded from the measurement in E112 but not in E2627 unless the data is to be compared to measurements previously made according to E112. The reader should note that this is in spite of the fact that misidentification of a boundary as a twin is less likely in EBSD data due to the crystallographic information, even though a twin cannot be unambiguously

identified in either case as both crystallographic orientation and boundary plane inclination must be known. Third, the average grain must contain at least 500 measurement points. Finally, the data must be "cleaned up" to remove poor observation points. The prescriptions for resolution for the average grain and exclusion of grains below a given size are not part of ASTM E1382[17], which supplements ASTM E112 with additional guidelines specifically for automated and semi-automated measurement of grain size on digital images. ISO 13067[18], the International Organization for Standardization counterpart to ASTM E2627, provides different guidelines than are given in the ASTM standard. In many cases, it is not immediately clear that the differences between the standards are reconcilable with one another. Key differences are highlighted in Table I.

Table I. Summary of main requirements contained in ASTM E2627, ISO 13067 and ASTM E0112

Requirement	**ASTM E2627**	**ISO 13067**	**ASTM E0112**
Data clean up	Required, no more than 10% of points changed.	Required, no maximum number of points changed.	N/A
Twin boundaries	Not excluded unless for consistency with ASTM E112.	Exclusion is up to user; twin defined as < 2° deviation from trace	Excluded
Minimum grain size	500 px	10px	N/A
Minimum number of grains	50 whole grains observable in field	Not given	50 grains measured (can be on edge)
Edge grains	Excluded	Excluded	Count as 1/2
Boundary definition	5° misorientation (recommended)	5-15° misorientation (chosen by user)	N/A
Resolution	Average grain at least 500 px	Step size results in >10 px lineal intercept across average grain	N/A
Reporting	$\bar{A}, G$	$\bar{L}$, $\bar{d}_c(\bar{A})$, $\overline{d_{feret}}$ allowed	G

EBSD grain size data has often been reported in the literature (both before and after the development of relevant standards) as the circle equivalent diameter of the measured grain areas, i.e. the measured area values are converted to the more intuitive units of distance by forcing circle equivalence. This method of reporting is emphasized in ISO 13067. Circle equivalent diameters are not directly comparable to lineal intercept length measurements, which are the same in 2D and in 3D, and are thus stereologically correct measurements that can accurately reflect properties of a 3D aggregate of grains. The circle equivalent section diameter, on the other hand, can at best only serve as a proxy parameter for the 3D aggregate. The mean lineal intercept is sometimes estimated from the circle equivalent diameter by again assuming circularity: the mean linear intercept of a set of circles is $\pi/4$ times their mean diameter. Since grain sections are not actually circular (they have corners due to the constraints imposed by space-filling), there is a systematic error between the true lineal intercept and any estimate that assumes circle equivalence. ISO 13067 recommends the following conversion between the mean lineal intercept and the circle equivalent diameter based on an empirical observation of aluminum and ferrous alloys measurements (in Annex A; original sources [18–21]):

$$\bar{L} = \frac{d_c(\bar{A})}{2}\sqrt{\pi} \tag{4}$$

where the circle equivalent diameter $d_c(\bar{A})$ is defined from the mean grain sectional area $\bar{A}$ (i.e. $\bar{A} = \frac{\pi}{4}\left(d_c(\bar{A})\right)^2$). Note that this estimate differs from that given in ASTM E112 by a factor of $1/\left(\sqrt{\pi/4}\right)$ due to its empirical nature.

C. Tomkeieff's Equation for Two-Dimensional Figures

There exists an *exact*, stereologically correct relationship between the mean section area $\bar{A}$ and the mean lineal intercept $\bar{L}$, known as the Tomkeieff relation [22,23]:

$$\bar{L} = \frac{\pi \bar{A}}{\bar{C}} \tag{5}$$

Where $\bar{C}$ is the mean perimeter of the section areas. Substitution of $d_c(\bar{A})$ for $\bar{A}$ in equation 5 makes a direct conversion between circle equivalent diameter and mean lineal intercept possible. A derivation of this relationship is provided in Appendix A. In practice, the challenge in using the Tomkeieff relation on a digital image comes from measurement of the grain perimeters. There are a couple interrelated problems. First, the simplest possible approach to calculating the boundary length for a regular grid at a given resolution is inaccurate: the total length of pixel edges bordering other grains is higher than the length of the smooth boundary separating the two grains due to the jagged shape. Second, increasing spatial resolution in the measurement changes the observed length of grain boundary, which resembles a problem of fractal geometry. Both circumstances may be inferred from inspection of Figure 1. Finally, drawing lines between adjacent pixels rather than taking the jagged path between them requires ordering the pixels, which is non-trivial computationally in cases when the grain section is not globally convex. This last situation amounts to a constrained traveling salesman problem, for which all available algorithms require significant computation time when faced with a system of hundreds to thousands of grains with an average number of perimeter pixels per grain likely on the order of 10^3.

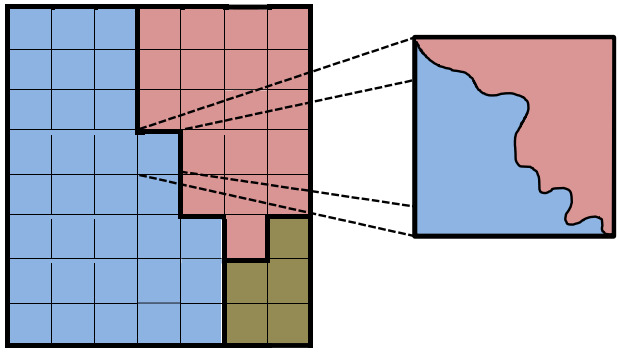

Figure 1. The magnification of a single pixel to a higher resolution can reveal hidden details about the grain perimeter path as illustrated.

D. Objectives

The ASTM grain size number has proven its usefulness in measuring grain sizes. However, the persistence of grain size reporting in terms of lineal intercepts and circle equivalent diameter show that there is also a distinct need for grain sizes to be reported in intuitive units. There also exists a need to be able to convert between the two values, or at least estimate one from the other. To the author knowledge, no previous work has addressed the application of Tomkeieff's equation for grain size measurements. There are two chief benefits to developing efficient grain perimeter estimation, enabling a direct conversion between grain areas measured by EBSD and lineal intercepts. First, such a technique would be applicable even in microstructures with elongated grains, such as those resulting from rolled, forged, or extruded metal products. In these microstructures, using lineal intercepts either requires precise alignment of the pixel row/column axes with the elongated direction of the grains (which can in fact be curved depending on the forming process) or repeated sampling with randomly oriented lines. Second, it would enable the usage of a stereologically correct parameter with intuitive units of distance for describing the grain size (i.e., avoiding the usage of circle equivalent diameter). Thus, the objectives of the present work are:

1. To present a microstructure simulation technique capable of efficient generation of realistic-looking microstructures with varied grain size dispersions and the ability to apply different pixel sampling resolutions to instances of the same microstructure;
2. To illustrate microstructural circumstances that create significant differences between results reported as circle equivalent diameter versus mean lineal intercept, and characterize these differences as a function of grain size dispersion;
3. To enable direct conversion between circle equivalent diameters and mean lineal intercepts by developing and calibrating a pattern-matching library, then comparing the use of such a library to alternative approaches to grain perimeter estimation already available in the literature;
4. To determine how various conversions between grain size measurement parameters are affected by imaging resolution and grain size dispersion, as well as

how much the ASTM grain size number estimated from a lineal intercept value deviates from one determined exactly from the mean grain area; and

5. To use observations to recommend best practices for reconciling differences between the relevant ASTM and ISO measurement standards.

EXPERIMENTAL PROCEDURE

A. Microstructure Simulation

To create model 2D microstructures on which the desired analyses could be performed, programs were written in Python 2.7. First, a lognormal distribution (when the logarithm of a variable presents a normal distribution) was randomly sampled to create a dispersion of discrete circle diameters. The list of circle diameters was sorted from large to small, and then an attempt was made to place each circle in a random location on a 2D map in such a way that it did not overlap any previously placed circles (one or more pixels of a circle taking the position of pixels of another circle). An example circle placement is shown in Figure 2(a) for a set of 30 circles with lognormally distributed areas, using a mean circle size of $250\ \mu m$, a lognormal shape parameter of 0.75, in a grid area of $22500\ \mu m^2$ and a volume fraction of ~20%. For all microstructure simulations, a maximum number of 100 failed attempts to place circles in the system was allowed. If this limit was reached with the given distribution parameters, the code would restart the circle placement process. Such a limit is necessary because certain selections of input parameters (such as a very broad distributions, or large mean intended circle sizes in a small grid area) result in either impossible or very time consuming attempts at circle placement within these rules.

The locations of the centroids of each circle were then repeated on a 3x3 grid, and taken as the nodes of a Voronoi diagram, as shown in Figure 2(b). The edges of the Voronoi tesselation extending out of the center box in the 3x3 grid were made to map to vertices on the opposite side, such that a system with toroidal boundary conditions could be created for input into Surface Evolver [24]. The obtained set of vertices, edges, and faces with toroidal boundary conditions is illustrated in Figure 2(c). Each system was run for a number of steps in Surface Evolver to reduce the interfacial energy of the system, creating a realistic-looking simulated grain structure with curved boundaries. This process is illustrated in Figure 2(d) and (e), which show the Surface Evolver input and output, respectively, for 1000 growth steps. The Surface Evolver outputs were then exported back into Python and mapped to a grid to simulate EBSD data, as shown in

Figure 2(f). Each pixel in the simulated EBSD map was assigned to a grain with a unique grain identifier number.

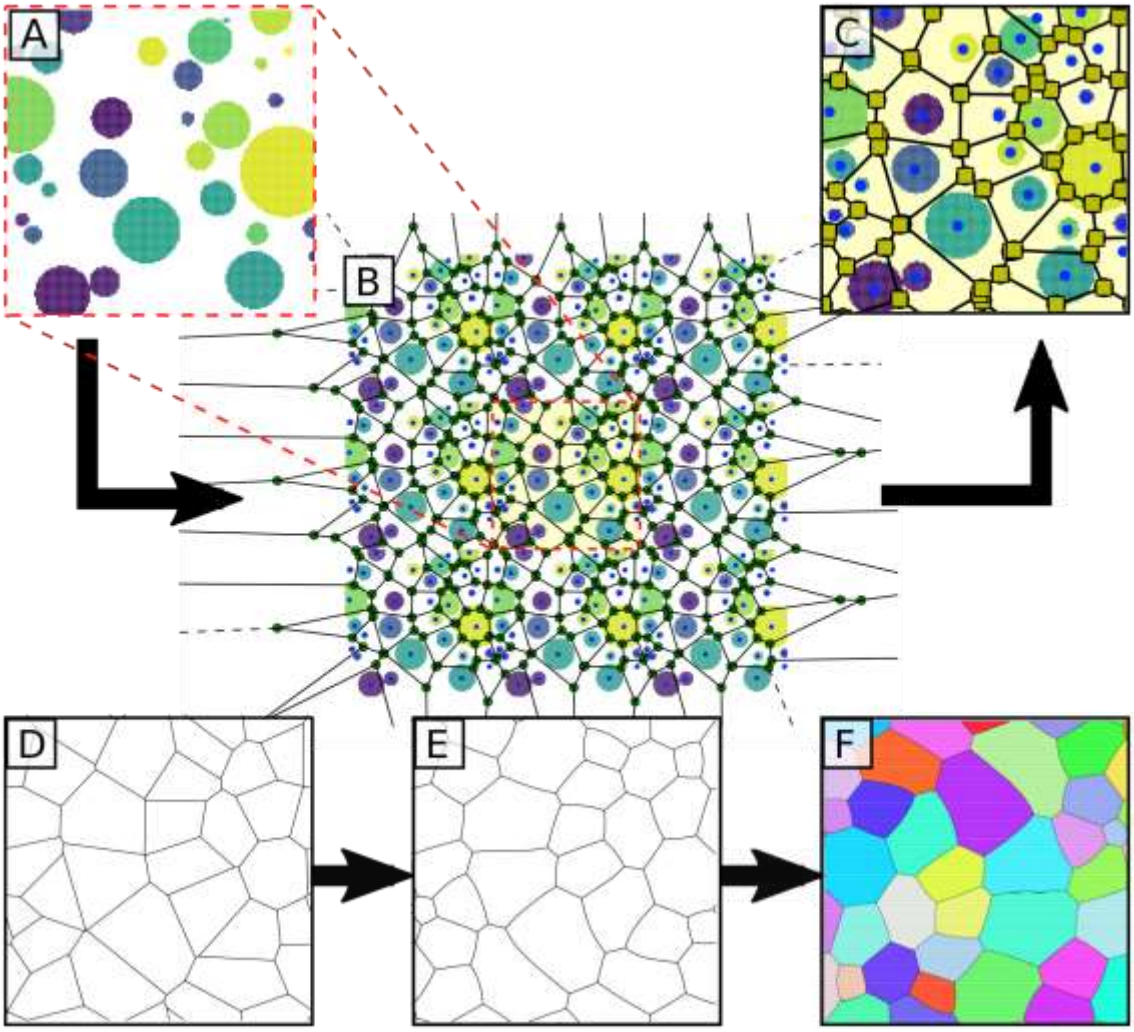

Figure 2. Illustration of the method used for simulation of EBSD data from a microstructurcture consisting of equiaxed grains of a single phase with varying dispersion of grain sizes. Circles with a lognormal distribution are placed in a 2D space(a) and subsequentially tiled in order to have a periodic condition (b). Which, the Voronoi diagram function (c) uses as input to generate a structure of space-filling vertices, edges and faces (d). The structure is then evaluated with Surface Evolver to obtain a microstructure (e) that can be fillied with simulated EBSD information (f).

The mean grain size after microstructure creation could be controlled by the "step size," a length value assigned to the distance between the pixels mapped onto the Surface Evolver results. The resolution defined, as *R* is the mean number of pixels per grain in the

simulated microstructure and also influences the final grain size. Figure 3 illustrates the difference obtained when mapping the Surface Evolver results to different step sizes, resulting in different resolution images of the same simulated grain structure. Figure 3(a) has an average of 150 px/grain while Figure 3(b) is exactly the same microstructure sampled with a finer step size such that it is rendered at a higher resolution with an average of 3000 px/grain.

Note that the input parameters of the microstructure simulation process employed here (c.f. Figure 2) do not directly reflect the resulting grain size dispersion. The microstructures present in this work were primarily identified by the measured arithmetic coefficient of variation CV (the ratio of the standard deviation to the mean value of the distributon) of the lineal intercept distribution and the number of grains in each microstructure. All simulated microstructures used for the analysis presented a larger number of grains than the ones shown for illustrative purposes in Figure 2 and Figure 3.

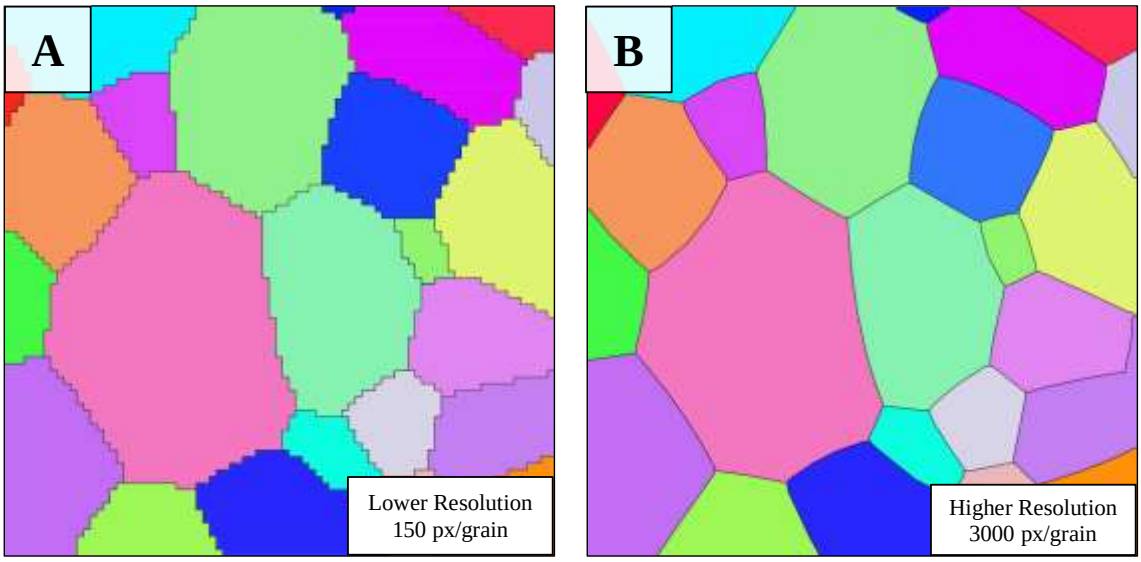

Figure 3. Illustration of the adjustment of step size mapped onto Surface Evolver results to simulate measurements of the same area at different resolutions.

To create a set of microstructures with varied grain size dispersions but similar resolutions and similar numbers of grains at the same "magnification," four basic parameters were systematically varied: the shape parameter of the circle size distribution σ, the intended mean circle area $\bar{A}_i$, the volume fraction V_f of placed circles and the

number of growth steps S. The system size for circle placement was held constant at 200 x 200 px. Values of 5, 10, 15, 20, and 25 px were used for $\bar{A}_i$, σ ranged from 0.01 to 2.0, and V_f ranged from 15 to 55%. Between 50 to 250 growth steps in Surface Evolver were used for each case.

B. Measurements

1. Mean Lineal Intercept

Following procedures contained in ASTM E112-10, an automated computational adaptation to Heyn's intercept method was written. Due to the simulated nature of the data analyzed, having no non-indexed pixels and a well-defined boundary, the regular procedure can be optimized to its limit in order to produce more accurate results. One by one, all vertical and horizontal lines of the microstructure are used as test lines. A single line column or row is isolated and its total length was calculated based on an assigned step size and the number of pixels covered. The individual intercept lengths were recorded as the number of pixels with a given unique grain identifier on that single line. Once all columns and rows were measured, the total number of intercepts was divided by the total length to obtain the mean lineal intercept $\bar{L}$.

2. Circle Equivalent Diameter

The mean circle equivalent diameter $\bar{d}_c(\bar{A})$ was measured based on the steps contained in the ISO 13067. The number of points belonging to each unique grain identifier was collected and multiplied by the area of a single pixel (e.g., the square of the step size in the case of square pixels). The mean value from all individual grain measurements was recorded as mean grain area $\bar{A}$. This information was then converted to a "circle equivalent diameter" using

$$d_c(\bar{\mathrm{A}}) = \left(\frac{\bar{A}}{(\pi/4)}\right)^{\frac{1}{2}} \tag{6}$$

Since the term "circle equivalent diameter" has been used in the literature to refer to different quantities, an alternative interpretation of the mean circle equivalent diameter of individual grain areas was also computed as:

$$\bar{d}_c(\mathrm{A}) = \frac{\sum_i^n \left(\frac{A_i}{\pi/4}\right)^{\frac{1}{2}}}{n} \tag{7}$$

3. Mean Perimeter

The real value of the perimeter can be either larger or smaller than that observed in a pixellated image, as illustrated in Figure 1. The simple approach to estimate the perimeter of an object in a digitized image is to observe only pixels in the boundary and count all edges exposed to the outside of the object. This value is then multiplied by the step size to calculate the simple perimeter P_s. Using this simple perimeter estimation approach, it is easy to see by inspection that the perimeter length measured on grains in Figure 3(a) would be higher than that measured on Figure 3(b), despite both images being from the same microstructure.

Another available estimate for object perimeter in digital images is that of Benkrid & Crookes [25], which assumes the way that the perimeter cuts through pixels in a square grid by taking into account the north, east, south, and west neighbor pixels and assigning a perimeter value of 1, $\sqrt{2}$, or $(1+\sqrt{2})/2$ to each case. It is this method that is implemented in the Scikit-Image module for image processing and analysis in Python [26]. Measurements of perimeter were performed with this method in addition to the aforementioned simple method for comparison to our custom-calibrated pattern matching library.

A customizable pattern matching library (PML) has the *potential* to more completely address the uncertainty about the behavior of the grain boundary under the pixel grid (cf. Figure 1) by assigning a statistically most probable boundary segment length. The curved boundary length that should be represented by a given pixel will vary with the resolution, as illustrated in the case of a spherical feature in Figure 4. Edge pixels of smaller features with higher boundary curvatures should generally contain

larger boundary lengths than larger features, even though both will exhibit the same pixel neighborhood patterns at the edges of the feature.

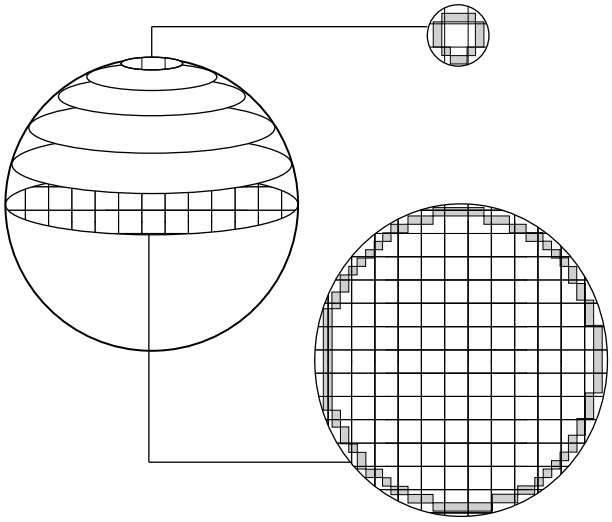

Figure 4. Illustration of the root cause of the variation in perimeter length represented by individual pixels and the relationship between that length and resolution, in the case of a spherical object.

Looking at each single pixel n in a grain, taking eight closest neighbors n_i for the square grid and six for hexagonal (as defined in Figure 5), it is conceivable to calculate all possible adjacent pixel neighborhood for that pixel; 256 neighboring pattern are possible on the square and 64 on the hexagonal grid.

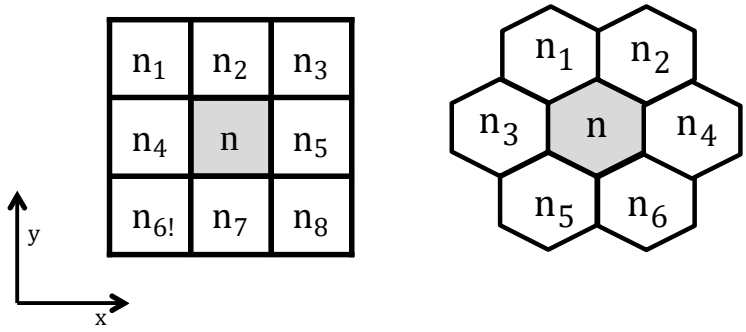

Figure 5. Square and hexagonal pixel grids common in EBSD data collection, and the neighbor numbering scheme used in the present work.

The relationship between the pixel row and column locations and the square grid neighborhood defined in Figure 5 is given in Table II.

Table II. Relationship between a pixel and its neighborhood in terms of row x and column y values in a square grid comprising the neighborhood vector N.

$n_1 = [x_n - 1\ ;\ y_n + 1]$ $n_4 = [x_n - 1\ ;\ y_n]$ $n_7 = [x_n\ ;\ y_n - 1]$	$n_2 = [x_n\ ;\ y_n + 1]$ $n_5 = [x_n + 1\ ;\ y_n]$ $n_8 = [x_n + 1\ ;\ y_n - 1]$	$n_3 = [x_n + 1\ ;\ y_n + 1]$ $n_6 = [x_n - 1\ ;\ y_n - 1]$
$N = (n_1, n_2, n_3, n_4, n_5, n_6, n_7, n_8)$		

The first step for creating such a library must be to build a table representing all possible neighboring patterns and assign a possible perimeter contribution value p for each of them, exemplified by Table III for the square grid case.

Table III. Schema representing how the complete pattern table was constructed, with all possible neighboring conditions and their respective perimeter contribution values, where n can be true and present ($n = 1$) or false and absent ($n = 0$).

Pattern #	n_1	n_1	n_1	n_1	n_1	n_1	n_1	n_1	Value
1	1	1	1	1	1	1	1	1	p_1
2	1	1	1	1	1	1	1	0	p_2
3	1	1	1	1	1	1	0	1	p_3
				.					
				.					
				.					
254	0	0	0	0	0	0	1	0	p_{254}
255	0	0	0	0	0	0	0	1	p_{255}
256	0	0	0	0	0	0	0	0	p_{256}

For sake of simplicity, and to enable direct comparison with the Benkrid & Crookes approach, the present work was performed exclusively with the square grid case. Using a number of 512 simulated microstructures as described in section 2.1, the probabilities of finding each neighborhood pattern were calculated to enable focused efforts on calibration of more critical p values. The symmetric equivalencies of the patterns in the library were determined to minimize the number of calibration values required.

To perform the perimeter measurement, each individual grain in the simulated EBSD data that did not border an edge was sequentially isolated, transforming the data into a binary map where the grain being measured has its identifier number converted to one while all other grains are reassigned to zero, then recording the information about the neighborhood of grain border pixels according to the indexation N present in the last row of Table II. For each pixel on the grain border, N is compared to the patterns table (cf. Table III), then a corresponding specific value p_i is assigned and multiplied by the step size as the representation of the perimeter segment trough that pixel. All p_i contributions are then summed to find the grain perimeter. The mean perimeter is determined after analysis of all grains that do not border the edge of the EBSD scan data. The versatility of this method stems from the potential for optimization of p_i values as they change with microstructure, in order to provide more accurate results.

Initial calibration of the library was performed by creating pixellated representations of circles with radii ranging between 0.501 and 50 in steps of 0.05 in arbitrary pixel units. For each border pixel of the circle, the length tangent line to the radius that fell within the pixel of interest was taken as an estimate of the perimeter segment that fell within that pixel. The mean of these perimeter segment values was taken for each pattern neighborhood N observed in the set of circles generated. Initial calibration values for patterns not matched by the pixellated circle were obtained by a similar procedure with a moon shape. It is known that one coordinate (for example, that on the *y-axis*) must be the same for the segments of the intersecting circles, such that $r_1 \sin\theta_1 = r_2 \sin\theta_2$. The required difference in x coordinate of the circle centers must be $r_2 \cos\theta_2 - r_1 \cos\theta_1$. Thus, the full range from a "slice of pie" (with a maximum size of a half moon) to a circle segment can be obtained with inputs of the radius of one circle and

a ratio of θ segment values between the two circles. Initial values for most of the remaining missing patterns for an initial calibration were obtained by determining mean length of tangent line segment falling within the pixel of interest for radii ranging from 0.501 and 50 in steps of 0.05 in arbitrary pixel units and theta ratios ranging from 0.05 to 0.95 radians in steps of 0.1. With these initial guesses for the p_i values, the calibration was refined using a sequential least square programming method [27] on the complete set of simulated microstructures to minimize the difference between the mean lineal intercept calculated from the Tomkeieff relation and the directly measured mean lineal intercepts. Fitting of an empirical equation to the calibration results as they changed as a function of resolution was performed using nonlinear least squares optimization in the SciPy module for Python.

RESULTS AND DISCUSSION

A. Simulated Microstructures Characteristics

A set of 512 simulated microstructures featuring a similar number of grains after the growth step was generated. The average number of non-edge grains in this set of simulated microstructure maps was 550. The number of grains ranged between 437 at the minimum and 592 at the maximum, with the standard deviation being 33.74 $\pm 10^{-2}$. Thus, the generated microstructures closely matched the 500 measured grains recommended in ASTM E2627 and exceeded the recommended number from ASTM E112 and ISO 13067. The Surface Evolver results were mapped onto pixel grids such that the number of pixels in the average grain ranged from 539 at the minimum to 754 at the maximum, with the mean being 608 and the standard deviation being 36.45 $\pm 10^{-2}$. Thus, all members of this set of simulated microstructures met the ASTM E2627 requirement of at least 500 px per grain. The CV of the intercept length distributions (i.e. the grain size dispersions) for the microstructures ranged from 0.64 to 0.88 with a median value of 0.74 (Figure 6).

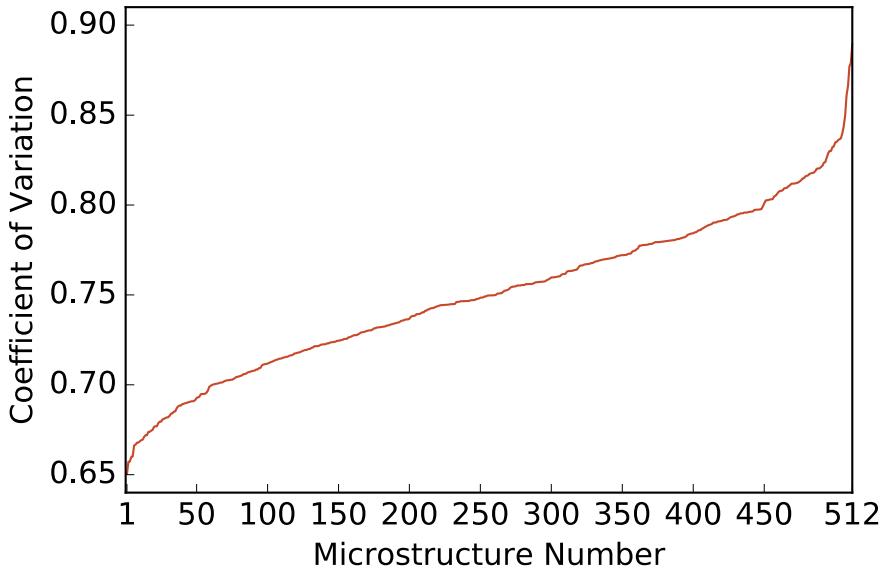

Figure 6. The ralation between each of the simulated microstructures and their respective CV, showing a concentration of microstructures around CV=0.75.

Published experimental work suggests that the grain volume-equivalent diameter is well described by the lognormal distribution down to very fine grain sizes[28]. In the present work, a lognormal distribution of 2D circle sizes was used as inputs, but this does not imply a lognormal distribution of grain section areas after Voronoi tesselation. The resulting distribution has a significant deviation from lognormality on the coarse grain tail in all cases and the fine grain tail has a lower probability than is characteristic for a lognormal distribution of 3D grain volumes, which is the opposite behavior of that expected for real grains. The uniform boundary energy in the Surface Evolver growth step used in the process will drive the grain size distribution shape toward that of the Hillert distribution shape[29], causing some of the microstructures to fit better to the normal distribution than the lognormal. The Hillert distribution skews in the opposite direction from those which are experimentally observed[30]. It is noticeable that upon increasing the number of growth steps the coefficient of variation also increases, indicating that the simulated microstructure state deviate from that required for normal, self-similar grain growth, and exhibiting higher tendency toward abnormal grain growth[30]. This is useful for obtaining a wide range of grain size dispersions but also serves as an indicator that the current generated microstructures may differ topologically from many real grain structures. Figure 7 compares the shape of a lognormal distribution and the distribution of grain size on a set of three representative microstructures with an average and extremes CVs on the first row, the second row presents a qualitative analysis of the grain size distribution to fit a lognormal distribution and the third row the same process was applied to a normal distribution.

While it is likely that the microstructures simulated through this work deviate from real microstructures both topologically and in terms of the grain size distribution shape, it is not expected to significantly change the probabilities of occurrence of specific 3x3 binary patterns appearing at the grain boundary, nor is it expected that this will heavily affect the calibration values since the calibration optimization was performed for a large number of microstructures with a wide range of grain size dispersions.

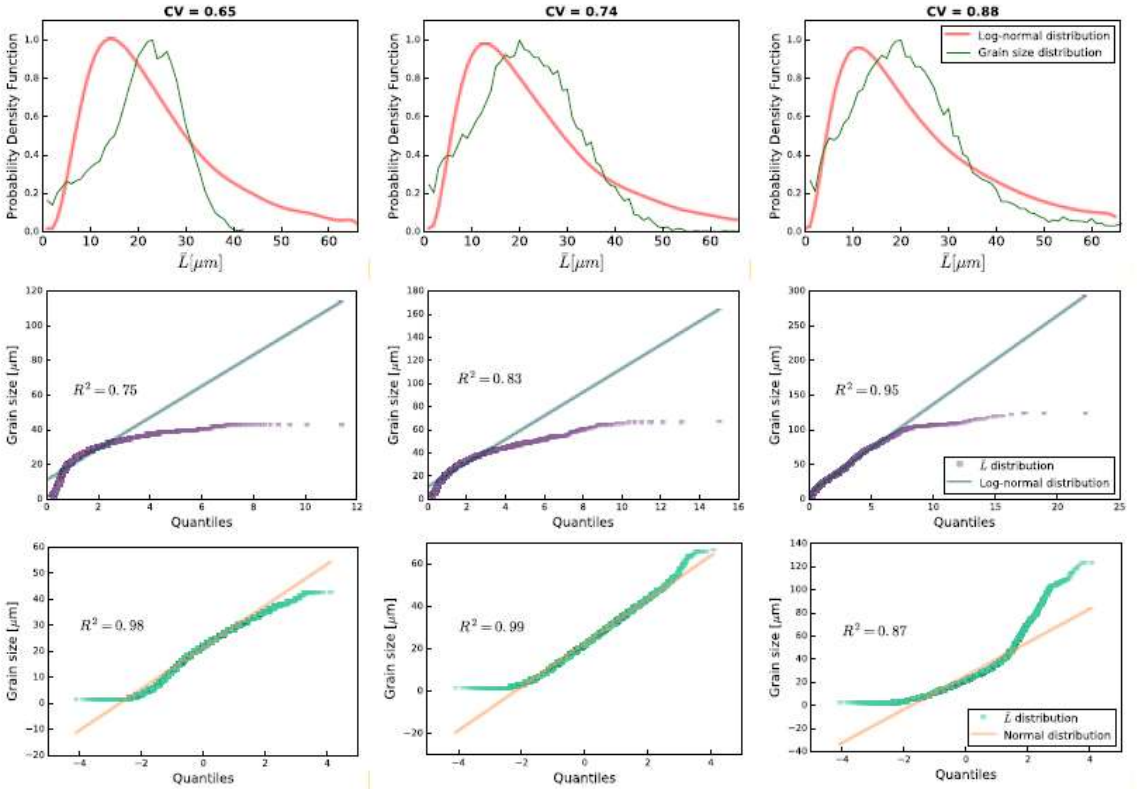

Figure 7. A Qualitative comparisson of three microstructures after Voronoi tesselation and Surface evolver grain griwth steps with varied CV, the first columns presentes data from a microstructure in the lower range of CV, the second columns from the average CV and the third from the upper range. The first row is a plot of probability density function of the grain size distribution and a lognormal distribution with equivalent parameters, the second row shows how well the data fits to a lognormal distribution and on the third row for a normal distribution.

The relationship between the input parameters and the resultant grain size distributions are exhibited in Figures 8, 9 and 10 In these figures, each point corresponds to one simulated microstructure, and is colored based on the number of growth steps used in Surface Evolver. Figure 8 shows the relationship between the mean areas of the placed circles and the mean areas of the resulting simulated grain sections (excluding those bordering an edge). It can be clearly seen that there is only a weak correlation between the input and output sizes, while there is a strong correlation between the number of growth steps in Surface Evolver and the output grain size. The weak correlation is due in part to the important role that the volume fraction input (which is not shown in the plot)

plays in the distance between the circle centers in the Voronoi diagram. The difference in scale between the x and y axes in the plot is due to the fact that the circle placement occurs on a different grid resolution from the mapping of the Surface Evolver results to the EBSD scan points: the output resolution is adjustable by changing the step size mapped onto the results.

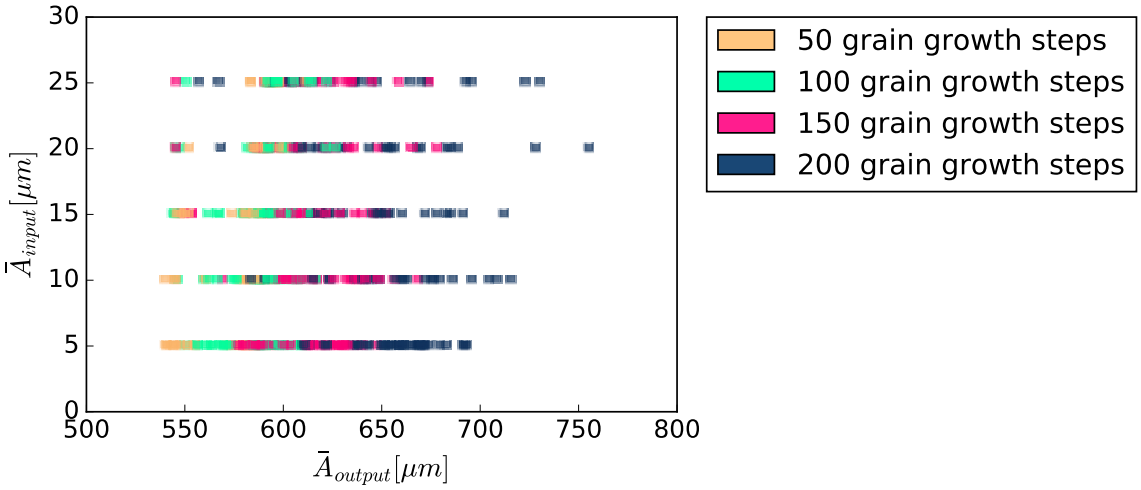

Figure 8. Relationship between input mean area of placed circles vs. mean area of resulting grains.

Figure 9 shows the correlation between the lognormal shape parameter of the lineal intercept distribution of input circles and the maximum likelihood estimate of the lognormal shape parameter of the resulting grain areas. In this case, it can be seen that there is a strong correlation between both the dispersion inputs for the circles and the dispersion of resulting grain sizes, with a consistent shift to the right as the number of growth steps in Surface Evolver increases. This implies that grain growth steps could be used as a parameter with strong influence to obtain structures with higher values of coefficient of variation of the grain size distribution. The scales on the x and y axes differ considerably, but a good estimate of the expected resultant dispersion of grain sizes can be obtained by taking into account both input $\hat{\sigma}$ and the number of growth steps.

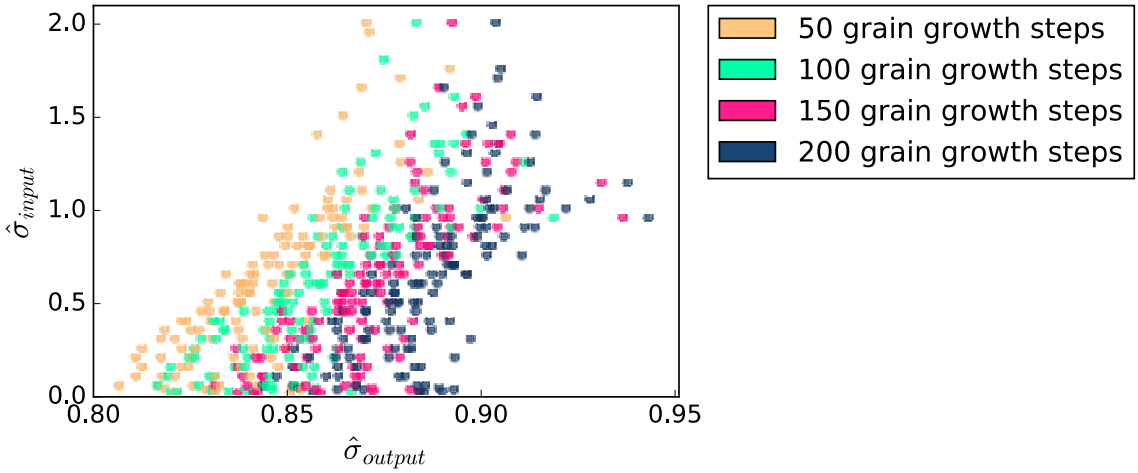

Figure 9. Input lognormal shape parameter vs. maximum likelihood estimation of the output lognormal shape parameter.

The relationship between the CV of the lineal intercept distribution of the simulated microstructures and the number of grains represented is shown in Figure 10. This shows that the number of Surface Evolver grain growth steps has a strong influence upon the number of features extinguishing smaller grains. This may help explain the dependence of the lognormal distribution shape parameter on the grain growth steps seen in Figure 9.

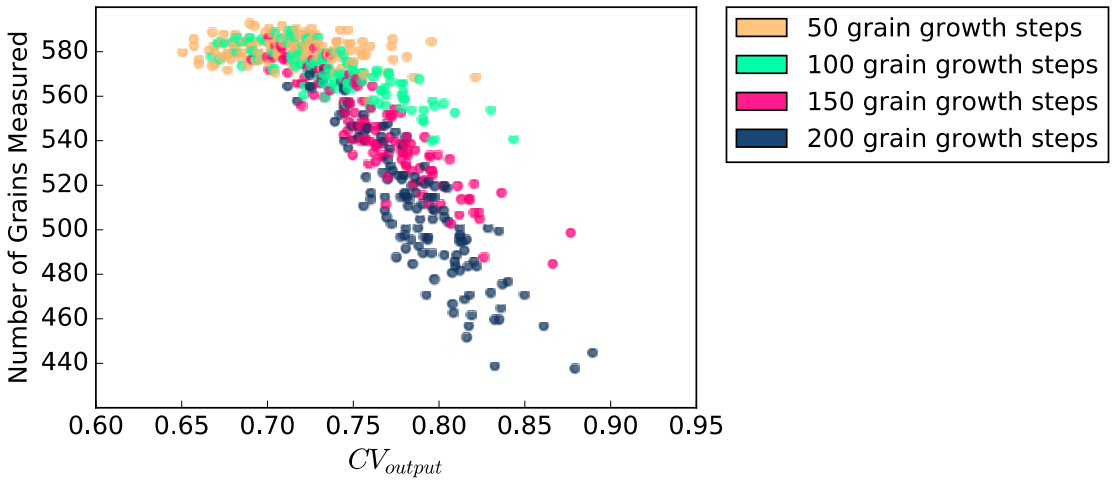

Figure 10. CV of the lineal intercept distribution of the simulated microstructures vs. the number of grains.

B. Grain Size Measurements

Figure 11 shows the mean lineal intercept and mean circle equivalent diameter (by two interpretations) of each microstructure plotted against CV. The circle equivalent diameters shown, $d_c(\bar{A})$ and $\bar{d}_c(A)$ were calculated according to Equations 6 and 7, respectively. It can be seen that the randomly generated set of microstructures exhibits a slight correlation between grain size and grain size dispersion, but that a very broad range of grain size dispersions has been obtained with a full range less than 6 µm, a mean lineal intercept of 21.7 ± 0.1 µm, and a standard deviation of 1.1 ± 0.1 µm. The circle equivalent diameters are in all cases larger than the corresponding mean lineal intercept value for a given microstructure. It is interesting to note that there is a slightly smaller range of values in the circle equivalent diameters than are observed in the lineal intercept results. The mean circle equivalent diameter value that was calculated by converting all individual grain areas, $\bar{d}_c$, exhibits a slight negative slope trend with increasing CV, opposite of what is observed with the mean lineal intercept and the circle equivalent diameter calculated from the mean area, $d_c(\bar{A})$ used in ISO 13067.

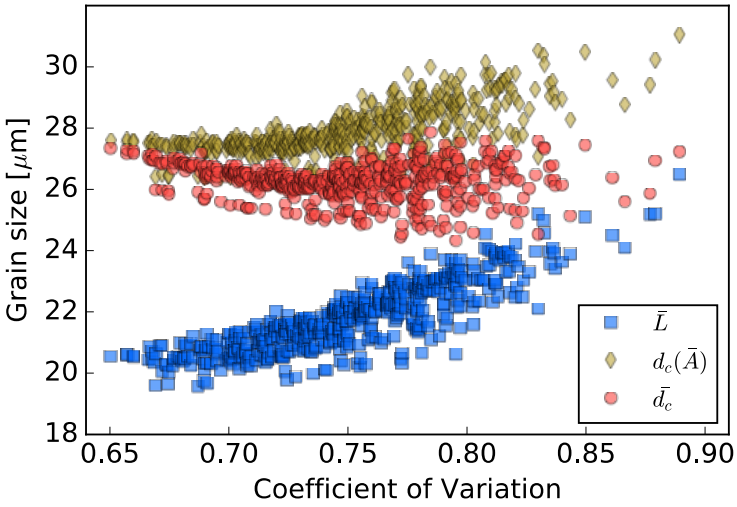

Figure 11. Comparison of mean lineal intercept and circle equivalent diameter grain size measurements for 512 simulated microstructures with different coefficients of variation *CV* of the lineal intercept distribution. The value $d_c(\bar{A})$ converts the mean grain area to a circle equivalent diameter while $\bar{d}_c$ converts each grain area to a circle equivalent diameter then takes the mean.

Using the circle equivalent diameter appears to have some distinct disadvantages relative to using lineal intercept to characterize the grain size in a material. It is not a stereological quantity and has no meaning in 3D – unlike lineal intercept or grain sectional area, both of which are the same in 2D as in 3D. Circle equivalent diameter only has intuitive meaning as a measurement of grain size for equiaxed microstructures. It is not clear how to interpret a "circle equivalent diameter" in a rolled microstructure when viewed, for example, along the transverse direction. These arguments have been made previously; however, the work performed here elucidates additional reasons why it might not be advisable to use the circle equivalent diameter: it changes more slowly as grain size dispersion changes than does the lineal intercept, capturing less detail about the diversity of grain shapes in the microstructure. Furthermore, there can be two interpretations of its meaning: the circle equivalent diameter of the mean grain sectional area ($d_c(\bar{A})$ in the present work) or the mean circle equivalent diameter of individual grain sectional areas ($\bar{d}_c(A)$ in the present work). In cases where the shape of the grain size distribution plays an important role in material processing or performance, the histogram of individual circle equivalent diameters has a mean that is different from that which should be used for conversion to alternative measurements of grain size, such as the ASTM grain size number. This interpretation also shows very little sensitivity to the grain size dispersion (as characterized by the lognormal coefficient of variation CV of the lineal intercept distribution), and in fact showed a slight decrease with increasing CV – opposite of the trend observed for lineal intercepts or the other interpretation of circle equivalent diameter. The existence of a difference between the mean circle equivalent diameter values is highly likely to be a source of confusion in reporting of results. Despite its drawbacks, the circle equivalent diameter does retain the strength of being an intuitive proxy for grain size as well as the benefit of being directly convertible to the ASTM grain size when the interpretation of the meaning of "circle equivalent diameter" is $d_c(\bar{A})$. The correct derivation for this direct conversion is given in Appendix B.

Figure 12 compares some interesting examples of the difference between mean lineal intercept and mean circle equivalent diameter measurements that were observed in the full set of microstructures generated. The grains have been arbitrarily assigned random orientations and colored according to a standard normal direction cubic inverse

pole figure scheme. The two microstructures in the top row have the same $d_c(\bar{A})$ but different $\bar{L}$ (CV increasing left to right, as indicated above each microstructure map), while the two microstructures in the bottom row have the same $\bar{L}$ but different $d_c(\bar{A})$ values (CV again increasing left to right). For the microstructures with the same $d_c(\bar{A})$, CV increases with increasing $\bar{L}$. In this particular example, for the microstructures with the same $\bar{L}$, CV increases with decreasing $d_c(\bar{A})$. This would not be expected to be generally the case, but it is consistent with the observations in Figure 11 where the $d_c(\bar{A})$ was observed to have a smaller dynamic range relative to $\bar{L}$. Another consequence of this difference in dynamic range is that a bigger difference in $\bar{L}$ could be observed in structures with similar values of $d_c(\bar{A})$ than vice versa.

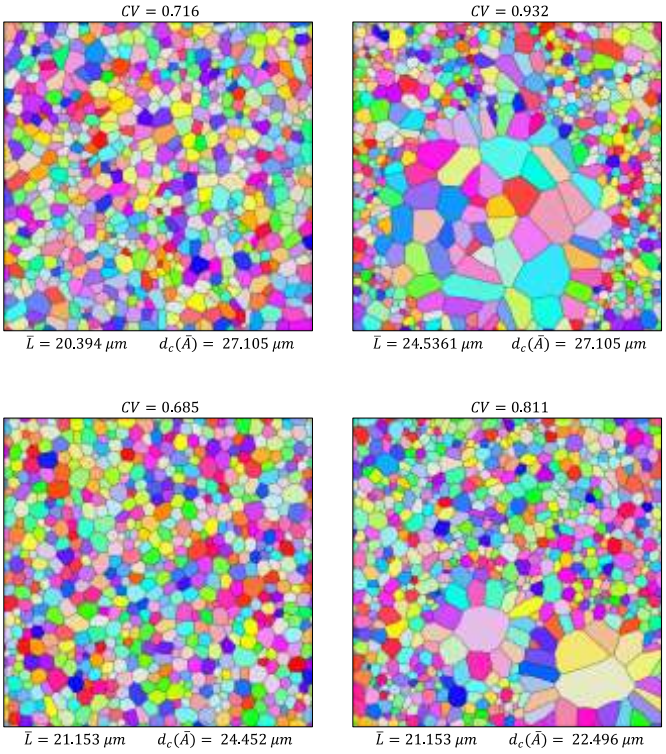

Figure 12. Example microstructures which show notable difference in either lineal intercept $\bar{L}$ or circle equivalent diameter $d_c(\bar{A})$. Top row: The same $d_c(\bar{A})$ but different $\bar{L}$ values; Bottom row: The same $\bar{L}$ but different $d_c(\bar{A})$ values. The coefficient of variation of the lineal intercept distribution is given above each microstructure map. Orientations of simulated grains are randomly assigned and colored according to a standard normal direction cubic inverse pole figure scheme.

C. Comparison of Grain Size Measurements from ASTM & ISO Standards

The difference between the ASTM grain size G calculated using the mean grain area (Equation 1) and the estimate using the mean lineal intercept (Equation 2) was characterized for the set of 512 simulated microstructures and is shown in Figure 13. The results suggest that estimating G from a lineal intercept measurement may produce an error as high as 3% for microstructures with either very low (~0.65) or very high (~0.90) CV values. For most of the generated microstructures the error was quite low: the absolute mean error was 0.002% with a standard deviation of 0.97% $\pm$ 0.01%. The error was minimized at a CV of 0.77. ASTM E112 notes that the Equation 2 estimate produces G values within 0.1 units of the 'correct' value determined by the planimetric method, Equation 1. In comparison, if one uses the circle estimate of $\bar{L}$ (Equation 3) corresponding to a value of $\bar{A}$ determined from Equation 1 it is found that the error in G increases from 0.11% at G=14 to 3% at G=0.5. Thus, from a practical perspective, it appears that a higher error can be expected in G estimated from a measured lineal intercept for very coarse grains with very broad or very narrow dispersions.

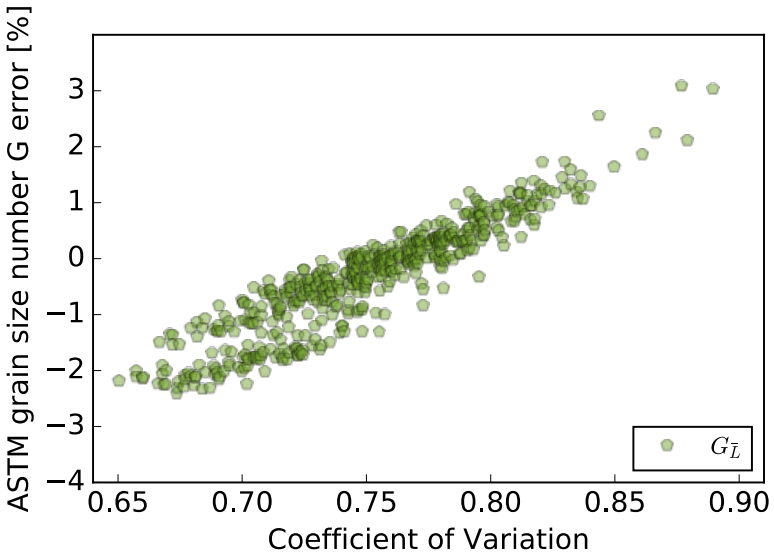

Figure 13. Error in ASTM grain size number estimated from lineal intercept measurements as a function of coefficient of variation of the lineal intercept distribution for 512 simulated microstructures.

The absolute values of measured mean lineal intercept $\bar{L}$ and estimates from the mean grain areas using equations from ASTM E112 ($\bar{L}_{ASTM}^{EST}$, Equation 3) and ISO 13067 ($\bar{L}_{ISO}^{EST}$, Equation 4) are compared in Figure 14. In both cases the conversion result is on average larger than the measured $\bar{L}$.

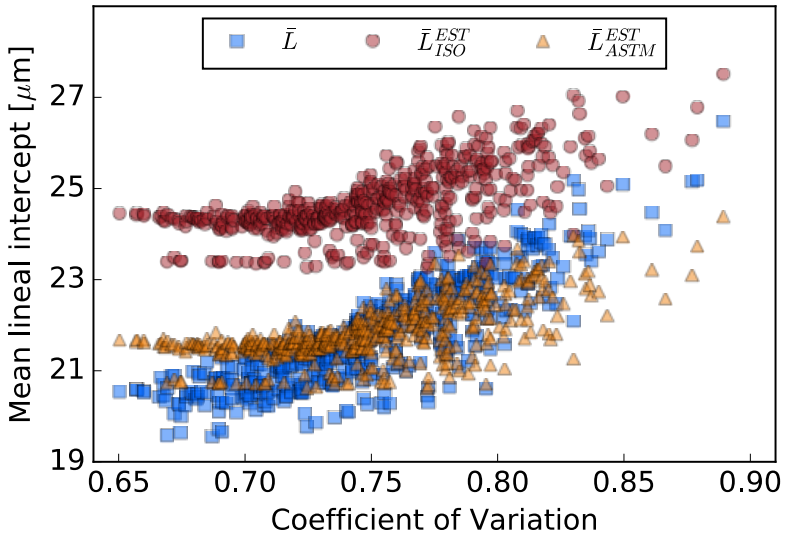

Figure 14. Comparison of measured mean lineal intercept and estimates of the mean lineal intercept calculated from mean grain areas using formulas in ASTM and ISO standards, as a function of the coefficient of variation of the lineal intercept distribution.

The conversion equation proposed by both ASTM E112-10 and ISO 13067 tries to find a solution for the issue of conversion between $d_c(\bar{A})$ and $\bar{L}$ with a unique estimate for each case. Through the analysis of the results it observed that the ASTM case performs significantly more accurately than the ISO case, but that the ASTM estimate has an increasing deviation from the correct lineal intercept result as the dispersion deviates from about 0.75 CV. The absolute error of the estimates relative to the measured $\bar{L}$ are shown in Figure 15. It can be clearly seen that the estimation using the Equation 3 shows a minimum error near the region of 0.75 CV where the great majority of the simulated microstructures are concentrated and that the performance Equation 4 improves at higher values of CV; however, both equations provide poorer results at low CV values.

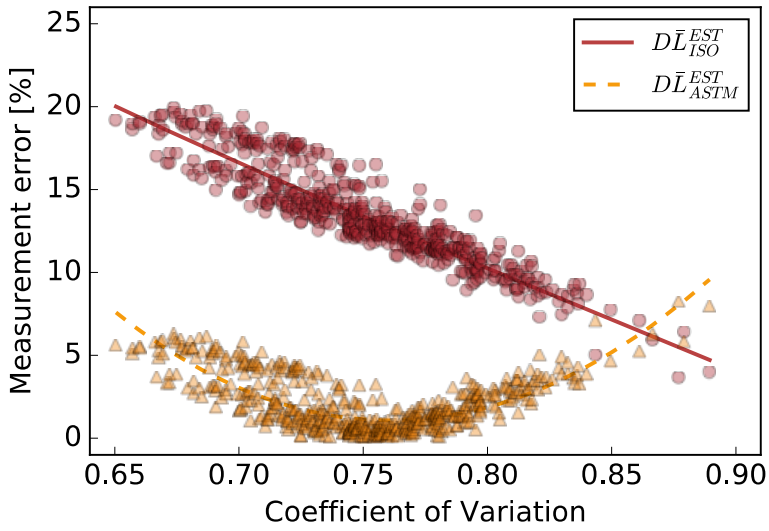

Figure 15. Error in estimated results relative to the measured lineal intercept.

ASTM E2627 calls for the use of a fine grain cutoff. This will affect the effective mean grain area, and thus result in a systematic error in the ASTM grain size number. Figure 16 shows the average effect on the mean grain area of imposing a cutoff of grains below a given threshold (on the x axis) on our simulated microstructures.

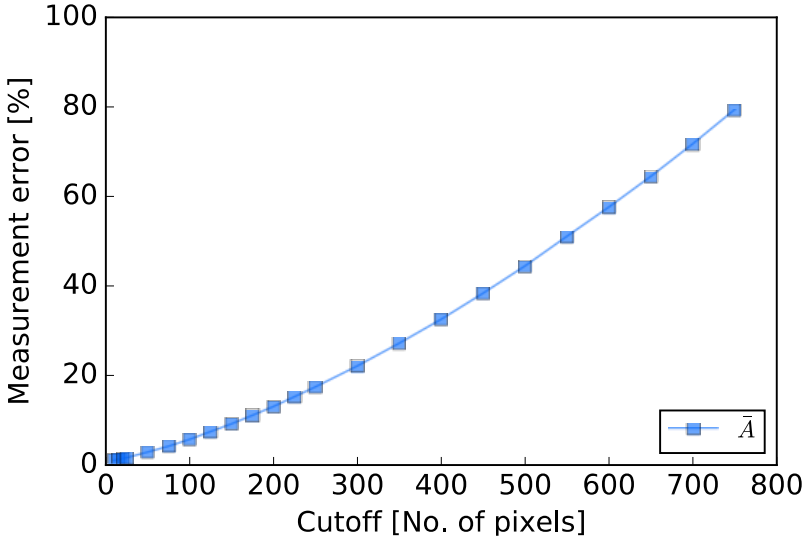

Figure 16. Error in mean grain area resulting from imposing a cutoff of fine grains below a given size threshold.

For measurements on microstructures slightly exceeding the prescribed resolution of 500 px in the average grain (such as our simulations), a removal of grain measurements with fewer than 100 px results in an average error in $\bar{A}$ of 4.65%. At this resolution, relatively small errors in the range of 0.59% to 0.04% are obtained for cutoffs below 25 px.

D. Pattern Matching Library Calibration

A first run of the pattern matching code on all available simulated microstructures provided information about the probability of occurrence of each pattern. Utilizing the symmetry of the patterns, it was possible to group the individual patterns to create a histogram of their probability of occurrence, as shown in Figure 17.

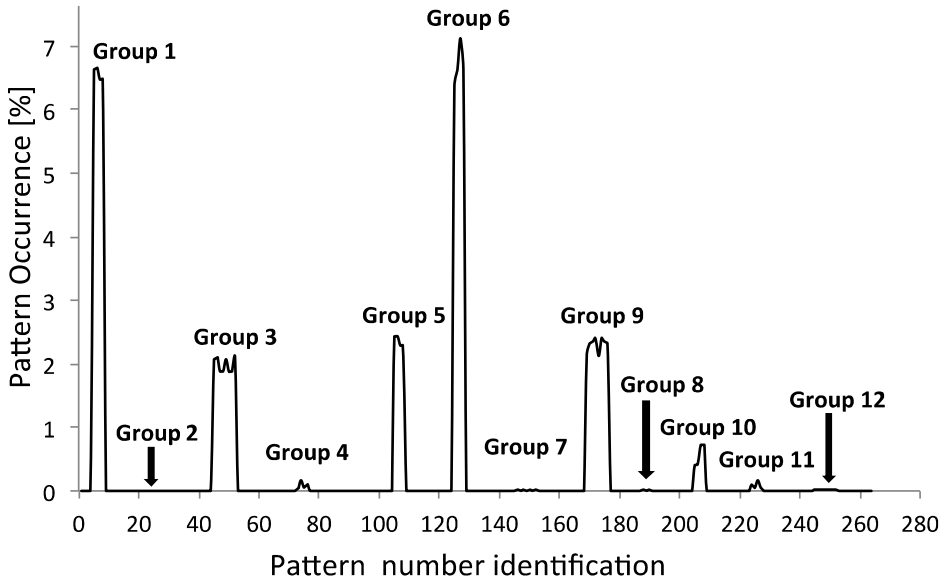

Figure 17. Histogram of frequency of occurrence of possible 3x3 pixel patterns (arbitrarily ordered by symmetric relationships) in the simulated microstructures. Twelve groups with distinguishable higher occurance are observed.

It was observed that it was impossible for some of the 256 theoretically possible patterns to occur due to the percolation technique commonly employed for grouping the measurement points into grains, and very unlikely for many of the patterns to occur in real measurements due to "cleanup" procedures that are frequently employed to remove unindexed or poorly indexed pixels. Only groups of patterns with total occurrence greater

than 0.01% were subsequently analyzed out of all 46 symmetrically equivalent and theoretically possible combinations of the 256 possible patterns. It was found that just 12 groups comprised more than 99.9% of all observed patterns in the simulated microstructure boundaries. This significantly reduced the number of patterns that needed a calibrated pattern perimeter contribution value p_i. The occurrence probability of each group, the symmetry, number of patterns and a graphic example of each of the 12 important groups are shown in Figure 18.

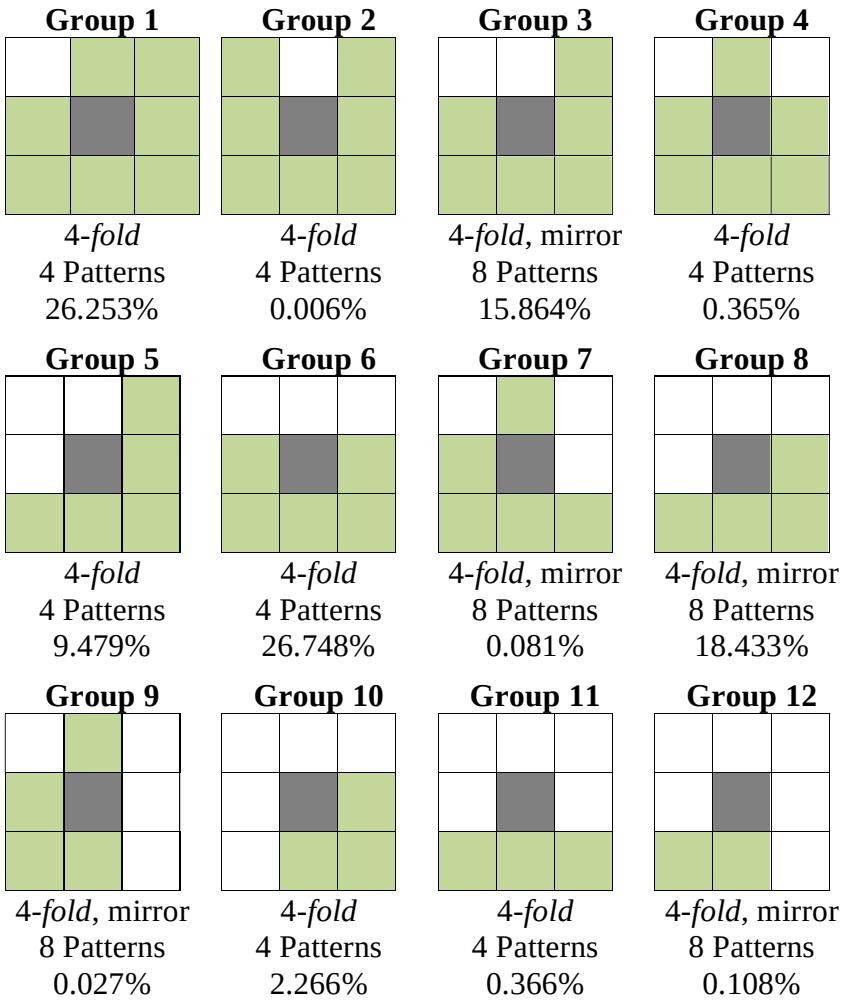

Figure 18. The twelve frequently occurring symmetrically related pattern groupings and their properties.

The result of the "initial guess" calibration with circles and moons was then assigned to each group of patterns, and the optimization routine was applied to all generated microstructures. Table IV shows all pattern indexations for all members of each group and the calibrated perimeter value after the optimization. Both groups one and four have been excluded from the table for not contributing with the perimeter since they do not show any exposed edge. These calibration values as well as the calibration values for all other possible patterns with very low probabilities of occurrence were assigned as zero.

Table IV. Optimized perimeter contribution values for the list of frequently occurring pattern groups, and the indexation of the members of each group.

Pattern group	Group patterns indexation	Perimeter Contribution
Group 2	[1,0,1,1,1,1,1,1] [1,1,1,1,1,1,0,1] [1,1,1,1,0,1,1,1] [1,1,1,0,1,1,1,1]	$p_{g2} = 2.371 \pm 10^{-3}$
Group 3	[0,0,1,1,1,1,1,1] [1,0,0,1,1,1,1,1] [1,1,0,1,0,1,1,1] [1,1,1,1,0,1,1,0] [1,1,1,1,1,1,0,0] [1,1,1,1,1,0,0,1] [1,1,1,0,1,0,1,1] [0,1,1,0,1,1,1,1]	$p_{g3} = 0.414 \pm 10^{-3}$
Group 5	[0,0,1,0,1,1,1,1] [1,1,1,1,0,1,0,0] [1,0,0,1,0,1,1,1] [1,1,1,0,1,0,0,1]	$p_{g5} = 1.553 \pm 10^{-3}$
Group 6	[0,0,0,1,1,1,1,1] [1,1,1,1,1,0,0,0] [1,1,0,1,0,1,1,0] [0,1,1,0,1,0,1,1]	$p_{g6} = 0.802 \pm 10^{-3}$
Group 7	[0,0,1,1,1,0,1,1] [1,0,0,1,1,1,1,0] [0,1,0,1,0,1,1,1] [1,1,1,1,0,0,1,0] [1,1,0,1,1,1,0,0] [0,1,1,1,1,0,0,1] [1,1,1,0,1,0,1,0] [0,1,0,0,1,1,1,1]	$p_{g7} = 0.631 \pm 10^{-3}$
Group 8	[0,0,0,0,1,1,1,1] [1,1,1,1,0,0,0,0] [1,0,0,1,0,1,1,0] [1,1,0,1,0,1,0,0] [0,1,1,0,1,0,0,1] [1,1,1,0,1,0,0,0] [0,0,0,1,0,1,1,1] [0,0,1,0,1,0,1,1]	$p_{g8} = 2.027 \pm 10^{-3}$

Group 9	[1,1,0,1,1,0,0,0] [0,1,1,1,1,0,0,0] [0,1,1,0,1,0,1,0] [0,1,0,0,1,0,1,1] [0,0,0,1,1,0,1,1] [0,0,0,1,1,1,1,0] [0,1,0,1,0,1,1,0] [1,1,0,1,0,0,1,0]	$p_{g9} = 0.566 \pm 10^{-3}$
Group 10	[1,1,0,1,0,0,0,0] [0,0,0,0,1,0,1,1] [0,1,1,0,1,0,0,0] [0,0,0,1,0,1,1,0]	$p_{g10} = 1.025 \pm 10^{-3}$
Group 11	[1,1,1,0,0,0,0,0] [0,0,0,0,0,1,1,1] [0,0,1,0,1,0,0,1] [1,0,0,1,0,1,0,0]	$p_{g11} = 1.427 \pm 10^{-3}$
Group 12	[1,1,0,0,0,0,0,0] [0,1,1,0,0,0,0,0] [0,0,1,0,1,0,0,0] [0,0,0,0,1,0,0,1] [0,0,0,0,0,0,1,1] [0,0,0,0,0,1,1,0] [0,0,0,1,0,1,0,0] [1,0,0,1,0,0,0,0]	$p_{g12} = 0.535 \pm 10^{-3}$

E. Pattern Matching Library & Tomkeieff Equation Results

The measurement error in the mean lineal intercept values calculated using the Tomkeieff relationship (Equation 5) is shown Figure 19 for each set of generated microstructures, as a function of the CV of the lineal intercept distribution.

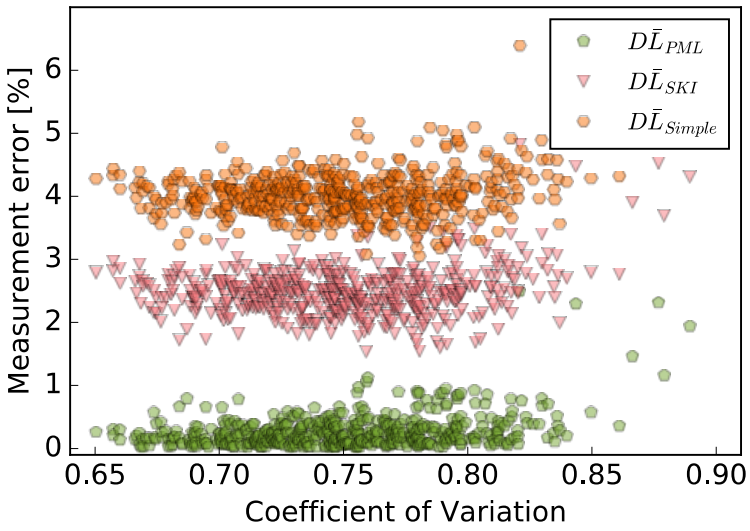

Figure 19. Performance of the calibrated pattern matching library in the Tomkeieff relationship relative to alternative perimeter estimations.

The error relative to the measured mean lineal intercept using the sum of the length of exposed edges of the pixels is plotted as $D\bar{L}_{Simple}$, the technique of Benkrid & Crookes is plotted as $D\bar{L}_{SKI}$, and the calibrated pattern matching library is plotted as $D\bar{L}_{PML}$. A lower global error is found with the pattern matching library $D\bar{L}_{PML}$ than is obtained using the alternative approaches.

The information collected from the boundary pixels is dependent on the resolution. Furthermore, it can contain overlapping diffraction pattern from more than one grain, which may be difficult to resolve using Hough transform-based indexing. Recent progress in dynamical EBSD pattern simulations may be helpful in more precise determination of the boundary location when necessary[31,32]. In most cases, one pattern is strong enough that an orientation can be assigned even if the signal from another orientation is present in the interaction volume. When the orientation cannot be assigned, image processing and cleaning techniques (as recommended by the ASTM and ISO standards, summarized in Table I) can be used to eliminate poorly indexed points. Thus the real shape and length is hidden as illustrated by Figure 1. To the author knowledge, the effect of missing and noisy data on EBSD grain size measurements is not well characterized in the literature.

The accuracy of all three perimeter estimation techniques was observed to vary with resolution (characterized here by the mean number of pixels per grain in the microstructure). A set of three representative microstructures (CV = 0.67, 0.71, and 0.83) were selected to study the behavior of the measurement when varying the resolution. The resolution was varied from an average number of px per grain of 18 up to 30000. The factor by which all perimeter calibration values in the pattern matching library must be multiplied to minimize the error in mean lineal intercept (as calculated using the Tomkeieff relationship) is plotted against resolution in Figure 20. For the calibration optimized for a resolution ~600 px per grain (cf. Table IV), the measurement error shows an oscillation in error behavior as resolution decreases. As resolution increases from the value for which the library was optimized, the error shows a stable increase with resolution and the results fit well to an arctangent equation, as given in the figure legend. The fit parameters shown were obtained using resolution values in the range of 102 to

2750 mean number of px per grain. The fit has a residual sum of squares of 3.2E-4 within this resolution range.

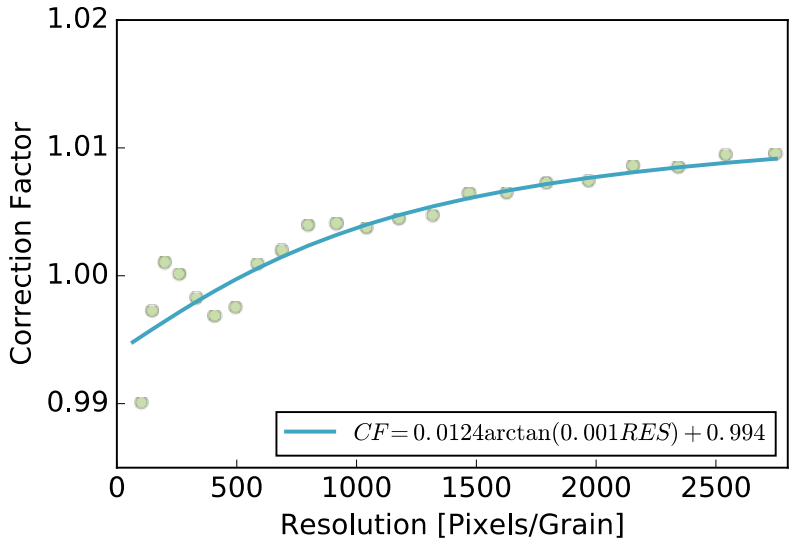

Figure 20. Multiplication factor for perimeter contribution values and Adjustment of pattern matching library with resolution, defined as mean number of measurement points per grain.

Figure 21 compares the results of the pattern matching library on the set of representative microstructures at different resolutions using this fit equation versus the 'uncorrected' library (i.e. the calibration values presented in Table IV) and the approach from Benkrid & Crookes. Each data point represents the mean error from the three representative microstructures. The points shown correspond to resolutions ranging from an average number of px per grain of 66 to 2750. It can be seen that the "resolution corrected" pattern matching library performs very well at a wide range of resolutions, but the performance rapidly becomes poorer below around an average of 100 px per grain. The error is 1.95% at 66px and was observed to increase rapidly below this resolution such that the data points were outside of the range shown in the plot. At resolutions in the range of 70-120 px in the average grain, it appears that the difference in performance between the Benkrid & Crookes approach and the pattern matching library are negligible. Furthermore, both are within the error expected from an experimental measurement.

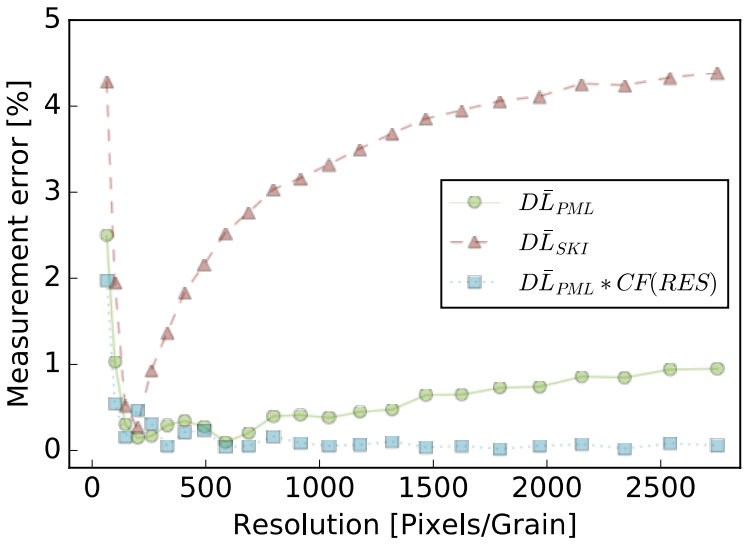

Figure 21. Performance of resolution-corrected pattern matching library compared to uncorrected and the perimeter estimation technique proposed by Benkrid & Crookes [24]

The mean measurement speed for the perimeter estimation methods were analyzed using a set of 10 randomly chosen microstructures with a representative mean resolution of 600 px/grain and 550 grains. Despite considering a 3x3 neighborhood rather than the four nearest neighbors on the square grid, the pattern matching library did not require significantly more computation time for perimeter estimation than either the "simple" or Benkrid & Crookes methods. The latter required an average of ~18 s per microstructure while both the pattern matching library and "simple" approaches required ~24 s running on a single core of a 2.5 GHz laptop computer. In comparison, the mean time necessary for the measurement of $\bar{A}$ on the same microstructures was equal to 0.3 sec.

SUMMARY AND CONCLUSIONS

Realistic-looking equiaxed microstructures with different grain size distributions but similar numbers of grains can be efficiently simulated using an approach that includes placement of a distribution of circles, Voronoi tesselation of the circle centroids, a growth step in SurfaceEvolver to minimize interfacial energies, and mapping of the Surface Evolver results to a pixel grid. The latter mapping step allows for any pixel resolution to be mapped onto the same microstructure results, making it possible to perform detailed studies of the effects of sampling resolution on grain size measurements. The primary drawback of this microstructure simulation method is that the input distribution parameters do not match the output parameters.

Very different microstructures may exhibit the same circle equivalent diameters with different mean lineal intercept grain sizes and vice versa. The mean lineal intercept has a larger dynamic range than circle equivalent diameter. The meaning and significance of lineal intercept measurements are less likely to be misinterpreted than circle equivalent diameter.

Circle equivalent diameter may be directly converted to ASTM grain size number, while the lineal intercept cannot. The error when estimating G from lineal intercept ranged up to 2% in the simulated microstructures, depending on grain size dispersion; however, it is centered about zero such that narrow grain size distributions appear to have a smaller G than they should and broad grain size distributions appear to have a larger G than is correct. The absolute error was minimized when the lognormal coefficient of variation of the lineal intercept distribution is around 0.75.

Symmetry and probability of occurrence reduce the 256 possible 3x3 binary pixel patterns to just 12 groups for which a calibration value is required to produce a pattern matching library for grain perimeter length estimation. Calibration values must scale with the resolution of the measurement but a very low error is obtainable by simply multiplying all calibration values in the library by a multiplication factor that is a function of resolution (rather than having a different library for each resolution). A pattern matching library approach to perimeter length estimation can produce significantly lower

perimeter measurement errors in the resolution range recommended by ASTM 2627 than alternative perimeter estimators if properly calibrated. The pattern matching library does not differ significantly in computation time than the simpler and less accurate perimeter estimation methods.

With an accurate perimeter estimation technique, the Tomkeieff relationship can be employed for calculating an unbiased mean lineal intercept directly from measurements of grain area. Lower errors are obtained across a wide range of grain size dispersions than the approximations recommended in the ASTM and ISO standards. For conversions in cases where the data is unavailable for measurement of the mean grain perimeter, making the assumption that equiaxed grains are approximately circular (as recommended by the ASTM standard) results in a generally low error, especially when the lognormal coefficient of variation of the lineal intercept distribution is close to 0.75.

FUTURE WORK

Accurate perimeter measurement is the challenge to overcome to be able to utilize the Tomkeieff equation. The challenge in creating a “one size fits all” perimeter length for a given pattern is that the fraction of smallest grains with higher curvatures represented by the pixels changes with the resolution. One possibility is to use a completely different calibration library for features of different sizes. In the present work, only the possibility of a calibration that varies with the resolution of the average grain was investigated. An empirical equation for a multiplication factor that can be used with the calibrated library results to give good perimeter estimations for resolutions in the range of 100 to 30000 px in the average grain was presented. The author believes that good estimates over a wider range of resolutions might be possible by accounting for the oscillations in the necessary multiplication factor. This might be done, for example, by summing the contributions from a power law and a nonlinear dampened harmonic oscillator (the “wavelength” of the oscillations appears to increase as resolution increases in Figure 20). A much larger number of resolutions would need to be studied in order to fit to such an equation due to the large number of function parameters.

The present work was only performed with square pixel grid. Many EBSD measurements are collected on a hexagonal grid, as shown in Figure 5 because the distances between the measurement points are then all the same (an arrangement which may be useful for misorientation-based analyses). The hexagonal grid has fewer possible patterns for a library. A library for the hex grid option was not developed because it would not have been possible to compare the results to the Benkrid & Crookes perimeter estimation already available in the literature [25]. It is assumed that an equivalent work can be executed with the hexagonal system, providing consistent results to those presented here.

A complete statistical and topological analysis of the simulated microstructures was outside of the intended aims and scope of this work investigations; however, a thorough comparison of the microstructure simulation approach presented here to others in the literature [33–36] would be an interesting direction for future studies. One clear benefit

of employing an external growth step is the possibility of achieving simulated microstructures with good topological agreement to real microstructures: It should be possible to extend this research approach to 3D and to include non-uniform grain boundary energies. The CMU mbuilder program also employs a growth step for obtaining a more realistic looking simulated microstructure [36]. Using a program like Surface Evolver (which operates on a list of faces, edges, and vertices) for the growth step has the benefit of making it easy to re-grid a resulting microstructure at any pixel or voxel resolution desired, with either a hexagonal or square scheme, in contrast to a grain growth simulation using a Monte Carlo or phase field approach that typically operates only on a voxel grid.

REFERENCES

1. E. O. Hall, "The Deformation and Ageing of Mild Steel: III Discussion of Results," *Proc. Phys. Soc. Sect., B,* **64** [9] 747–753 (1951).

2. N. J. Petch, "The Cleavage Strength of Polycrystals," *J Iron Steel Inst Lond.,* **173** 25–28 (1953).

3. B. Wilshire and C. J. Palmer, "Grain size effects during creep of copper," *Scr. Mater.,* **46** [7] 483–488 (2002).

4. O. D. Sherby and E. M. Taleff, "Influence of grain size, solute atoms and second-phase particles on creep behavior of polycrystalline solids," *Mater. Sci. Eng. A,* **322** [1] 89–99 (2002).

5. S. L. Semiatin, J. M. Shank, A. R. Shiveley, W. M. Saurber, E. F. Gaussa and A. L. Pilchak, "The Effect of Forging Variables on the Supersolvus Heat-Treatment Response of Powder-Metallurgy Nickel-Base Superalloys," *Metall. Mater. Trans. A,* **45** [13] 6231–6251 (2014).

6. E. A. Prokofiev, J. A. Burow, E. J. Payton, R. Zarnetta, J. Frenzel, D. V. Gunderov, R. Z. Valiev and G. Eggeler, "Suppression of Ni4Ti3 Precipitation by Grain Size Refinement in Ni-Rich NiTi Shape Memory Alloys," *Adv. Eng. Mater.,* **12** [8] 747–753 (2010).

7. D. Morrison, "Effects of grain size on cyclic plasticity and fatigue crack initiation in nickel," *Int. J. Fatigue,* **19** [93] 51–59 (1997).

8. X. Cui, Y. Wu, X. Liu, Q. Zhao and G. Zhang, "Effects of grain refinement and boron treatment on electrical conductivity and mechanical properties of AA1070 aluminum," *Mater. Des.,* **86** 397–403 (2015).

9. H. Pan, Z. Zhang and J. Xie, "The effects of recrystallization texture and grain size on magnetic properties of 6.5 wt% Si electrical steel," *J. Magn. Magn. Mater.,* **401** 625–632 (2016).

10. N. Wang, Z. Wang, K. T. Aust, and U. Erb, "Effect of grain size on mechanical properties of nanocrystalline materials," *Acta Metall. Mater.,* **43** [2] 519–528 (1995).

11. L. Wang, E. Mostaed, X. Cao, G. Huang, A. Fabrizi, F. Bonollo, C. Chi, and M. Vedani, "Effects of texture and grain size on mechanical properties of AZ80 magnesium alloys at lower temperatures," *Mater. Des.,* **89** 1–8 (2016).

12. K. Zhou, B. Liu, Y. Yao and K. Zhong, "Effects of grain size and shape on mechanical properties of nanocrystalline copper investigated by molecular dynamics," *Mater. Sci. Eng. A,* **615** 92–97 (2014).

13. "Standard Test Methods for Determing Average Grain Size," ASTM Designation E 112-13. American Society of Testing and Materials, West Conshohocken, PA.

14. E. Heyn, "Short reports from the metallurgical laboratory of the Royal Mechanical and Testing Institute of Charlottenburg," *Metallographist,* **5** 37–64 (1903).

15. J. E. Hilliard, "Estimating grain size by the intercept method," *Met. Prog.*, **85** 99–102 (1964).

16. "Practice for Determining Average Grain Size Using Electron Backscatter Diffraction (EBSD) in Fully Recrystallized Polycrystalline Materials," ASTM Designation E 2627-13. American Society of Testing Materials, West Conshohocken, PA.

17. "Standard Test Methods for Determining Average Grain Size Using Semiautomatic and Automatic Image Analysis," ASTM Designation E 1382-15. American Society of Testing and Materials, West Conshohocken, PA.

18. "Microbeam analysis -- Electron backscatter diffraction -- Measurement of average grain size," ISO Designation 13067-11. International Organization for Standardization, Geneva, Switzerland.

19. H. W. L. Phillips, "The Grain Size of Rolled Aluminum," *J Inst Met.,* **58** 47–108 (1942).

20. F. Schückher and L. Janerot, "Kornstorlekbestämningsmetoder," *Jernkontorets Ann,* **143** 593–614 (1959).

21. R. T. Dehoff and F. N. Rhines, *Quantitative microscopy, 1st ed.;* pp. ?-?. McGraw-Hill, New York, NY, 1968.

22. E. E. Underwood, *Quantitative stereology, 1st ed.*; pp. ?-?. Addison-Wesley, Boston, MA, 1970.

23. S. I. Tomkeieff, "Linear Intercepts, Areas and Volumes," *Nature* **155** [24] 24–24 (1945).

24. K. A. Brakke, "The Surface Evolver," *Exp. Math.,* **1** [2] 141–165 (1992).

25. K. Benkrid and D. Crookes, "Design and FPGA Implementation of a Perimeter Estimator," *Ir. Mach. Vis. Image Process. Conf.,* 51–57 (2000).

26. S. Van der Walt, J. L. Schönberger, J. Nunez-Iglesias, F. Boulogne, J. D. Warner, N. Yager, E. Gouillart, and T. Yu, "Scikit-image: image processing in Python," *PeerJ.*, **2** 453 (2014).

27. D. Kraft, "A software package for sequential quadratic programming," (1988).

28. J. C. Tucker, L. H. Chan, G. S. Rohrer, M. A. Groeber and A. D. Rollett, "Comparison of grain size distributions in a Ni-based superalloy in three and two dimensions using the Saltykov method," *Scr. Mater.,* **66** [8] 554–557 (2012).

29. P. R. Rios and M. E. Glicksman, "Polyhedral model for self-similar grain growth," *Acta Mater.,* **56** [5] 1165–1171 (2008).

30. E. J. Payton, G. Wang, M. J. Mills and Y. Wang, "Effect of initial grain size on grain coarsening in the presence of an unstable population of pinning particles,". *Acta Mater.,* **61** [4] 1316–1326 (2013).

31. G. Nolze, A. Winkelmann and A. P. Boyle, "Pattern matching approach to pseudosymmetry problems in electron backscatter diffraction," *Ultramicroscopy,* **160** 146–154 (2016).

32. Y. H. Chen, S. U. Park, D. Wei, G. Newstadt, M. A. Jackson, J. P. Simmons, M. DeGraef and A. O. Hero, "A Dictionary Approach to Electron Backscatter Diffraction Indexing," *Microsc. Microanal.,* **21** [3] 739–752 (2015).

33. L. St-Pierre, E. Héripré, M. Dexet, J. Crépin, G. Bertolino and N. Bilger, "3D simulations of microstructure and comparison with experimental microstructure coming from O.I.M analysis," *Int. J. Plas.,* **24** [9] 1516–1532 (2008).

34. Z. Fan, Y. Wu, X. Zhao and Y. Lu, "Simulation of polycrystalline structure with Voronoi diagram in Laguerre geometry based on random closed packing of spheres," *Comput. Mater. Sci.,* **29** [3] 301–308 (2004).

35. J. C. Tucker, L. H. Chan, G. S. Rohrer, M. A. Groeber and A. D. Rollett, "Tail Departure of Log-Normal Grain Size Distributions in Synthetic Three-Dimensional Microstructures," *Metall. Mater. Trans. A,* **43** [8] 2810–2822 (2012).

36. S. D. Sintay and A. D. Rollett, "Testing the accuracy of microstructure reconstruction in three dimensions using phantoms," *Model. Simul. Mater. Sci. Eng.,* **20** [7] (2012).

APPENDIX

A. Derivation of Tomkeieff relation for conversion between circle equivalent diameters and lineal intercepts

Two well-known stereological relationships that are valid for any aggregates are $\bar{L} = 2\bar{V}/\bar{S}$ and $\bar{A} = \bar{V}/D$, where $\bar{L}$ is the mean lineal intercept, $\bar{V}$ is the mean particle volume, $\bar{S}$ is the mean particle surface area, $\bar{A}$ is the average area of interception of the particles,

$$\bar{L} = \frac{4D\bar{A}}{\bar{S}} \tag{1}$$

This relationship is not immediately useful as written because it would require prior knowledge of the mean caliper diameter of the particles and the mean surface area. A less appreciated relationship – but still one universally valid for globally convex particles – is $\bar{C} = \pi\bar{S}/4D$, where $\bar{C}$ is the mean perimeter length of the section areas of the particles and the other terms are as previously defined. Rearranging, we can obtain

$$\frac{1}{\bar{S}} = \frac{\pi}{4D\bar{C}} \tag{2}$$

Inserting Eq. (2) into Eq. (1), we obtain

$$\bar{L} = \frac{\pi\bar{A}}{\bar{C}} \tag{3}$$

Thus, a more reasonable estimate of the mean lineal intercept from the mean circle equivalent diameter would be:

$$\bar{L} = \frac{\pi^2\bar{d}^2}{4\bar{C}} \tag{4}$$

As a check on this result, it is worth noting that we can insert $C = \pi d$ (for circle equivalents) into the above equation and obtain $L = \pi d/4$, which is exactly Eq. 2.8 from ASTM E112 A2.2.2. The above equation shows a reduction in the mean lineal intercept as the perimeter length increases while the equivalent diameter is held constant, as we would expect from an increase in the number of corners of grains (i.e. more triple points existing in cross-section).

B. Derivation of the Conversion from Circle Equivalent Diameter to ASTM Number

The conversion between ASTM grain size number and circle equivalent diameter is given incorrectly in ISO 13067:2011. The ASTM grain size number G is formally defined as

$$N_{AE} = 2^{G-1} \tag{1}$$

Where N_{AE} is the number of grains per square inch at 100X magnification. There are 25.4 mm in one inch, so the number of grains per square mm at 1X+ is given by $N_{AE} = N_A \left(\frac{25.4}{100}\right)^2$. Rearranging for G and converting to SI units of mm at 1X, one obtains

$$G = \log_2(0.254^2 N_A) + 1 \tag{2}$$

The area of the average grain is related to the number of grains per unit area as $\bar{A} = 1/N_A$. Therefore, we can write

$$G = 2\log_2 0.254 - \log_2 \bar{A} + 1 \tag{3}$$

Defining the circle equivalent diameter $d_c(\bar{A})$ such that $\bar{A} = \frac{\pi}{4}\left(d_c(\bar{A})\right)^2$, we obtain:

$$\begin{aligned} G &= 2\log_2 0.254 - \log_2\left(\frac{\pi(d_c(\bar{A}))^2}{4}\right) + 1 \\ &= [2\log_2 0.254 - \log_2 \pi + 1 + \log_2 4] - [2/\log_{10} 2] \cdot \log_2\left(d_c(\bar{A})\right) \\ &= 2.6057 - 6.643856 \log_{10} d_c(\bar{A}) \end{aligned} \tag{4}$$

Where $\bar{d}$ is in mm at 1X. Note that the constant differs from that given in ISO 13067:2011. Using a similar procedure, one obtains

$$G = 17.32587 - 6.643856 \log_{10} d_c(\bar{A}) \tag{3}$$

for $d_c(\bar{A})$ in μm at 1X.